Numerical operator method for the real-time dynamics of strongly correlated quantum impurity systems far from equilibrium

Pei Wang, Guy Cohen, and Shaojun Xu

Phys. Rev. B **91**, 155148 — Published 28 April 2015

DOI: 10.1103/PhysRevB.91.155148

Numerical operator method for the real time dynamics of strongly-correlated quantum impurity systems far from equilibrium

Pei Wang,[1] Guy Cohen,[2,3] and Shaojun Xu[4]

[1] *Department of Physics, Zhejiang University of Technology, Hangzhou 310023, China**
[2] *Department of Chemistry, Columbia University, New York, New York 10027, U.S.A.*
[3] *Department of Physics, Columbia University, New York, New York 10027, U.S.A.*
[4] *School of Economics and Management, Zhejiang Sci-Tech University, Hangzhou 310018, China*

(Dated: February 17, 2015)

We develop a method for studying the real time dynamics of Heisenberg operators in strongly-interacting nonequilibrium quantum impurity models. Our method is applicable to a wide range of interaction strengths and to bias voltages beyond the linear response regime, works at zero temperature, and overcomes the finite-size limitations faced by other numerical methods. We compare our method with quantum Monte Carlo simulations at a strong interaction strength, at which no analytical method is applicable up to now. We find a very good coincidence of the results at high bias voltage, and in the short time period at low bias voltage. We discuss the possible reason of the deviation in the long time period at low bias voltage. We also find a good coincidence of our results with the perturbation results at weak interactions.

PACS numbers: 73.63.Kv, 72.10.Fk, 02.60.-x

I. INTRODUCTION

Understanding strongly-correlated open quantum impurity systems is an important unsolved problem in condensed matter physics, and is relevant to a wide variety of experimental fields. In cases ranging from molecular electronics junctions,[1–6] low-dimensional mesoscopic systems[7–9] and out-of-equilibrium correlated materials,[10–12] a need exists for reliable theoretical treatments which go beyond linear response from equilibrium. The combination of correlated quantum physics and the lack of a description in terms of equilibrium statistical mechanics presents a major challenge in this regard, and while a variety of powerful approximate schemes have been developed,[13–23] the entire spectrum of interesting parameters is not reliably covered by these methods. This makes numerically exact results highly desirable; however, even when one is interested only in the properties of a stationary state, the only recourse which does not involve approximations is often to consider time propagation from some simple initial state to the nonequilibrium steady state. Moreover, in some cases one can observe a system's time-dependent response to a quench,[24–27] and thus a theoretical treatment capable of following the system's time evolution is needed.[20,28–33]

A great deal of progress has been made by considering the special case of nonequilibrium quantum impurity models, where transport between sets of infinite, trivial, noninteracting leads occurs through a finite, nontrivial, interacting region.[7,34,35] The nonequilibrium Anderson model, where the dot is modeled as a single spin-degenerate electronic level with on-site Coulomb interaction, exhibits a range of exotic phenomena related to Kondo physics[36] and has drawn a particularly great deal of attention. While this model and its extensions are still an infinite many-body problem and remain under active research even at equilibrium,[36–42] the local nature of the interactions in impurity models results in major simplifications, and in recent years a great deal of progress has been made in the development of numerically exact methods which solve for transport properties in impurity models.[43–62] These controlled methods remain limited in their applicability; in particular, quantum Monte Carlo (QMC) methods[45,51,55] are generally slow to converge at low temperatures and long times, while time-dependent density matrix renormalization group (tDMRG)[49,50] and numerical renormalization group (NRG)[44,63] methods are effectively limited to systems where the leads can be efficiently mapped onto reasonably short 1D chains with a small site dimension, in such a way that entanglement along the chain remains low. In recent years, impurity models have also been of interest as auxiliary systems in the study of large or infinite interacting lattices, by way of the DMFT approximation.[64–66]

It is therefore necessary to continue exploring new numerical methods. In this regard, the following observation is of some interest: when studying real time dynamics, it is possible to solve the Schrödinger equation and obtain the evolution of quantum states. However, quantum states contain all the information about a quantum system, most of which is redundant when one is only interested in very few or even a single observable. An alternative route is to solve the Heisenberg equation and obtain the evolution of a specific observable operators. Solving the Heisenberg equation may allow for some simplification or optimization. We note that similar ideas have been discussed in the context of tDMRG, where matrix product operators can be more efficient for describing dynamics than matrix product states.[67–72] The entanglement area laws which make DMRG perform so well for the ground states of gapped systems, however, do not extend to nonequilibrium situations and metallic systems. It is not therefore clear that tDMRG should be an optimal scheme for such systems as impurity models.

We propose a different approach: to express the solution of the time-dependent observable operators, we construct a set of basis operators, similar to how one might choose basis vectors in the Hilbert space. As will be shown, we can choose the basis operators so that the observable that we are interested in is itself a basis operator at time zero. The time-dependent observable operator then starts from a point on an axis of the operator space and explores the other dimensions at a finite rate, thus facilitating an efficient evaluation of the time evolution in our basis. This allows us to work with an infinite model and circumvent finite-size effects.

In this paper, we develop a numerical operator method (NOM) for nonequilibrium quantum impurity models, based on previous work by one of the authors.[73,74] We apply the method to the real time transport dynamics of the Anderson impurity model. Our method is in principle applicable to arbitrary bias voltage and interaction strength. It describes infinite reservoirs (which are difficult within tDMRG) at absolute zero temperature (which is difficult for QMC), and can therefore be expected to be advantageous in some regimes. We compare our results with perturbation theory at weak interactions and with QMC at strong interactions. We find perfect coincidence in most cases where it is expected, and discuss possible reasons for deviations in problematic regimes.

The contents of the paper are arranged as follows. In sec. II, we introduce the model and the preliminary transformation of the Hamiltonian. In sec. III, we show the details of the NOM. In sec. IV, we show the validity and power of our method by giving some examples and comparing our method with the others. At last, a concluding section summarizes our results.

II. THE MODEL AND THE TRANSFORMATION OF THE HAMILTONIAN

A. The Anderson impurity model

The NOM is designed for solving the Heisenberg equation of motion. In this paper, we discuss its application to the study of transport through the nonequilibrium Anderson impurity model, an archetypal model for the description of electron-electron interactions in quantum junctions.[75] The model involves an impurity site coupled to two ("left" and "right") electronic reservoirs or leads:

$$\hat{H} = \sum_{k,\alpha,\sigma} \epsilon_k \hat{c}^\dagger_{k\alpha\sigma}\hat{c}_{k\alpha\sigma} + \frac{g}{\sqrt{2}} \sum_{k,\alpha,\sigma} \left(\hat{c}^\dagger_{k\alpha\sigma}\hat{d}_\sigma + H.c.\right) + \hat{H}_{imp}. \tag{1}$$

Here $\hat{d}_\sigma$ is an electronic annihilation operator at the impurity, while $\hat{c}_{k\alpha\sigma}$ is an electronic annihilation operator in the reservoirs. $\alpha \in \{L, R\}$ denotes the left and right reservoir, respectively, $\sigma \in \{\uparrow, \downarrow\}$ denotes the spin and k is an index corresponding to a reservoir level with energy ϵ_k. g describes the coupling strength between the impurity and the reservoirs (taken to be level-independent here). $\hat{H}_{imp}$ is the local Hamiltonian at the impurity site, and is expressed by

$$\hat{H}_{imp} = \epsilon_d \sum_\sigma \hat{d}^\dagger_\sigma \hat{d}_\sigma + U \hat{d}^\dagger_\uparrow \hat{d}_\uparrow \hat{d}^\dagger_\downarrow \hat{d}_\downarrow, \tag{2}$$

where ϵ_d is the level energy and U is the Coulomb interaction. We concentrate on the particle-hole symmetric point $\epsilon_d = -U/2$ throughout the paper. We further define the impurity level broadening $\Gamma = \rho\pi g^2$ (ρ denoting the density of states of the reservoir). As is customary in the field, Γ will be used as the unit of energy.

We assume an infinitely sharp cutoff in the reservoirs at a finite bandwidth D. It is worth noting that our method can in principle be used for an arbitrary frequency-dependent coupling $\Gamma(\omega)$. We work at zero temperature, and take the chemical potentials of the left and right reservoirs to be $\mu_L = V/2$ and $\mu_R = -V/2$, respectively; V is therefore a bias voltage across the junction. At large V, the system is driven beyond the linear response regime and can no longer be described well in equilibrium terms.

B. The Wilson transformation

We will not directly apply the NOM to the Hamiltonian Eq. (1), but instead begin by discretizing the system and mapping it onto a one-dimensional chain with only nearest-neighbor couplings by way of a Wilson transformation. The reason for this is one of numerical efficiency: the NOM works well when each creation and annihilation operator appears in only a few terms of the Hamiltonian. In the transformed Hamiltonian, this is true for operators either at the impurity site or on the Wilson chain. However, in the original Hamiltonian Eq. (1), the operator $\hat{d}_\sigma$ appears in an infinite number of terms of the form $\left(\hat{c}^\dagger_{k\alpha\sigma}\hat{d}_\sigma + H.c.\right)$, since the infinite reservoirs must be described by an infinite (or at least large) number of k indices. We note that the Wilson transformation, which entails logarithmic discretization, is not a unique choice in this regard: a more general Lanczos transformation allows for arbitrary discretization schemes, and has been successfully employed in performing similar mappings, for example in the context of recent DMRG[41] and configuration interaction[42] solvers for equilibrium impurity models. It should also be mentioned that the Wilson transformation used was employed within the time-dependent numerical renormalization group (tNRG) method to access the real time dynamics of quantum impurity models coupled to both a single bath[43] and multiple baths.[63] We mention briefly that within the method described in this work, the logarithmic discretization of the Wilson chain suppresses the growth of the basis we will employ compared to a uniform discretization, thus resulting in improved computational efficiency.

To proceed, it is useful to recombine the field operators in the two reservoirs into pairs $\hat{c}_{k\pm\sigma} = \frac{1}{\sqrt{2}}\left(\hat{c}_{kL\sigma} \pm \hat{c}_{kR\sigma}\right)$, where $\hat{c}_{k+\sigma}$ is called the symmetric operator and $\hat{c}_{k-\sigma}$ the antisymmetric operator. The Hamiltonian is then divided into symmetric and antisymmetric parts: $\hat{H} = \hat{H}_+ + \hat{H}_-$, where

$$\hat{H}_- \equiv \sum_k \epsilon_k \hat{c}^\dagger_{k-\sigma}\hat{c}_{k-\sigma} \tag{3}$$

and

$$\hat{H}_+ \equiv \sum_k \epsilon_k \hat{c}^\dagger_{k+\sigma}\hat{c}_{k+\sigma} + g\sum_{k,\sigma}\left(\hat{c}^\dagger_{k+\sigma}\hat{d}_\sigma + H.c.\right) + \hat{H}_{imp}. \tag{4}$$

The symmetric Hamiltonian describes an impurity coupled to a single band, and can be transformed into a Wilson chain by a logarithmic discretization of the band. Following ref. 36, we then have

$$\begin{aligned}\hat{H}_+ =& \hat{H}_{imp} + \sqrt{\frac{\Gamma D}{\pi}}\sum_\sigma\left(\hat{d}^\dagger_{0\sigma}\hat{d}_\sigma + H.c.\right) \\ &+ \sum_{n=0}^{\infty} t_n\left(\hat{d}^\dagger_{n\sigma}\hat{d}_{n+1,\sigma} + H.c.\right),\end{aligned} \tag{5}$$

where $\hat{d}_{n\sigma}$ with $n = 0, 1, \cdots$ denotes the field operator on the Wilson chain, Γ the impurity level broadening, D the bandwidth of the reservoir, and t_n the coupling between neighboring sites on the chain. For constant Γ, an analytical expression for the coupling strength can be obtained:

$$t_n = \frac{D}{4}\frac{\left(1+\Lambda^{-1}\right)\left(1-\Lambda^{-n-1}\right)}{\sqrt{1-\Lambda^{-2n-1}}\sqrt{1-\Lambda^{-2n-3}}}\Lambda^{-n/2}, \tag{6}$$

where $\Lambda > 1$ is a discretization parameter.

Finally, the full Hamiltonian consists of the combination of the antisymmetric part and the Wilson chain, which are commutative with each other. It can be expressed as

$$\begin{aligned}\hat{H} =& \sum_k \epsilon_k \hat{c}^\dagger_{k-\sigma}\hat{c}_{k-\sigma} + \hat{H}_{imp} + \sqrt{\frac{\Gamma D}{\pi}}\sum_\sigma\left(\hat{d}^\dagger_{0\sigma}\hat{d}_\sigma + H.c.\right) \\ &+ \sum_{n=0}^{\infty} t_n\left(\hat{d}^\dagger_{n\sigma}\hat{d}_{n+1,\sigma} + H.c.\right).\end{aligned} \tag{7}$$

In the limit $\Lambda \to 1$, the transformed Hamiltonian Eq. (7) is equivalent to the original Hamiltonian Eq. (1). We can therefore fully eliminate the error caused by the Wilson transformation by taking the limit $\Lambda \to 1$. It has been argued[76] that the Wilson chain is not a thermal reservoir due to a finite heat capacity, which scales as $1/\ln\Lambda$ in the limit $\Lambda \to 1$, such that the temperature of the Wilson chain is not fixed in a transport setup. However, the dissipated energy in the setup within a finite time is also finite, such that the chains simulate true reservoirs for any given finite time if Λ is close enough to 1. Due to the fact that the NOM operates on a set of truncated Heisenberg-picture operators, the length of the Wilson chain does not significantly impact the computational scaling and can essentially be taken to infinity (see Fig. 1 and the corresponding discussion there). It can therefore be expected that it be valid to study the dynamics up to some finite timescale even after a Wilson transformation with $\Lambda > 1$. In practice, for the timescales explored here, we find that setting $\Lambda = 1.2$ is sufficient for converging the discretization error. We have verified that further reducing Λ to 1.02 does not significantly modify the results; we further note that within standard tDMRG this is generally difficult to achieve and often values of $\Lambda \simeq 2$ are used.[76]

III. THE NUMERICAL OPERATOR METHOD

A. The current operator

We study the current $I(t) \equiv \left\langle \hat{I}(t) \right\rangle$ through the impurity at a finite bias voltage V. The current operator is given by

$$\hat{I}(t) = -\frac{ig}{2}\sum_{k,\sigma}\left(\hat{d}^\dagger_\sigma(t)\,\hat{c}_{k-\sigma}(t) - H.c.\right), \tag{8}$$

where we have employed the antisymmetric field operators $\hat{c}_{k-\sigma}(t)$ in order to express the difference between the currents as measured in the left and right reservoirs. We assume that the reservoirs and the impurity site are initially decoupled from each other. The two reservoirs begin in their respective equilibrium states as determined by the Fermi distribution $f_\alpha(\epsilon_k) = \theta(\mu_\alpha - \epsilon_k)$, while the impurity site is empty. We switch on the coupling g at $t = 0$ and track the time evolution of the current. Since $\left[\hat{H}_+, \hat{c}_{k-\sigma}\right] = 0$, it is straightforward to find that $\hat{c}_{k-\sigma}(t) = e^{-i\epsilon_k t}\hat{c}_{k-\sigma}$. We therefore introduce a new field operator $\hat{c}_{-\sigma} = \frac{1}{\sqrt{\rho}}\sum_k e^{-i\epsilon_k t}\hat{c}_{k-\sigma}$, and re-express the current as

$$I(t) = 2\sqrt{\frac{\Gamma}{\pi}}\mathrm{Im}\left\langle \hat{d}^\dagger_\sigma(t)\,\hat{c}_{-\sigma}\right\rangle. \tag{9}$$

The problem is therefore reduced to the calculation of $\hat{d}^\dagger_\sigma(t)$, which will be addressed by computational means in the following subsection.

B. Iterative solution of the Heisenberg equation of motion

To obtain the time dependence of $\hat{d}^\dagger_\sigma$, we solve the Heisenberg equation of motion

$$\frac{d\hat{d}^\dagger_\sigma(t)}{dt} = i\left[\hat{H}, \hat{d}^\dagger_\sigma(t)\right]. \tag{10}$$

Since the antisymmetric Hamiltonian $\hat{H}_-$ commutes with $\hat{d}^\dagger_\sigma$, this becomes

$$\frac{d\hat{d}^\dagger_\sigma(t)}{dt} = i\left[\hat{H}_+, \hat{d}^\dagger_\sigma(t)\right]. \tag{11}$$

The symmetric Hamiltonian $\hat{H}_+$ describes a semi-infinite Wilson chain with the impurity site as its first site. To simplify the notation, we relabel the impurity site index as -1 such that the impurity annihilation operator is $\hat{d}_{-1,\sigma} \equiv \hat{d}_\sigma$. The symmetric Hamiltonian is then

$$\begin{aligned}\hat{H}_+ =& \epsilon_d \sum_\sigma \hat{d}^\dagger_{-1,\sigma}\hat{d}_{-1,\sigma} + U\hat{d}^\dagger_{-1,\uparrow}\hat{d}_{-1,\uparrow}\hat{d}^\dagger_{-1,\downarrow}\hat{d}_{-1,\downarrow} \\ &+ \sum_{\sigma,n=-1}^{\infty} t_n\left(\hat{d}^\dagger_{n\sigma}\hat{d}_{n+1,\sigma} + H.c.\right),\end{aligned} \tag{12}$$

where $t_{-1} \equiv \sqrt{\frac{\Gamma D}{\pi}}$.

In order to express $\hat{d}^\dagger_{-1,\sigma}(t)$, we construct a set of basis operators. At each site $j = -1, 0, \ldots$, we choose some linearly independent set of sixteen local operators generated by $\hat{d}^\dagger_{j\sigma}$ and $\hat{d}_{j\sigma}$ and including the unit operator. These are denoted by $\hat{\omega}^i_j$ for $i \in \{1, 2, \ldots, 16\}$, and every operator acting only on site j can be expressed as a linear combination of the sixteen $\hat{\omega}^i_j$. We then propose that a basis operator $\hat{O}_\alpha$ in the full symmetric subspace be expressed as the product of on-site operators in an ascending order:

$$\hat{O}_\alpha = \prod_{j=-1}^{\infty} \hat{\omega}^{\alpha_j}_j. \tag{13}$$

Here α is an aggregate index representing a vector α_j with $j \in \{-1, 0, 1, \ldots\}$, which identifies the basis element in the full operator Hilbert space. The basis $\left\{\hat{O}_\alpha\right\}$ is complete in the sense that any operator can be decomposed as a linear combination of its members. Additionally, the coefficients of this decomposition are unique.

In the basis just described the solution of the Heisenberg equation Eq. (11) can be written as

$$\hat{d}^\dagger_\sigma(t) = \sum_\alpha a_\alpha(t)\,\hat{O}_\alpha. \tag{14}$$

In tDMRG terms, one might say that our operator is represented by a sum of terms of bond order 1, which is clearly very different from a matrix product operator. To obtain the coefficient $a_\alpha(t)$ corresponding to each basis operator $\hat{O}_\alpha$, we derive an iterative equation by propagating from time t to time $t+\Delta t$ (where Δt is some small time interval) by using the forward Euler method:

$$\hat{d}^\dagger_\sigma(t+\Delta t) = \hat{d}^\dagger_\sigma(t) + i\Delta t\left[\hat{H}, \hat{d}^\dagger_\sigma(t)\right] + O\left(\Delta t^2\right). \tag{15}$$

We throw out terms of $O\left(\Delta t^2\right)$ and above, a valid approximation in the limit $\Delta t \to 0$. Next, substituting Eq. (14) into Eq. (15), we obtain

$$\hat{d}^\dagger_\sigma(t+\Delta t) = \sum_\alpha a_\alpha(t)\,\hat{O}_\alpha + i\Delta t\sum_\alpha a_\alpha(t)\left[\hat{H}, \hat{O}_\alpha\right]. \tag{16}$$

Calculation of the commutator $\left[\hat{H}_+, \hat{O}_\alpha\right]$ is trivial and easily computerized. The important point is now that at every stage of the computation, each $\hat{O}_\alpha$ appearing in the expansion with a nonzero coefficient can be written as the product of a finite number of (non-unit) local operators. Meanwhile, each term in the Wilson Hamiltonian Eq. (12) involves at most four local operators which act either at the same site or at two adjacent sites. Therefore, even though the Hamiltonian $\hat{H}_+$ contains an infinite number of terms, the commutator $\left[\hat{H}_+, \hat{O}_\alpha\right]$ is always finite in length for any finite $\hat{O}_\alpha$. In fact, $\left[\hat{H}_+, \hat{O}_\alpha\right]$ generates only very few terms when $\hat{O}_\alpha$ is short, as is the case when the propagation time t is not too large. That the commutator between the Hamiltonian and the basis operator contains a finite number of terms is a necessary condition in order for the NOM to be applicable. This condition can generally be satisfied for lattice models with only short-ranged interactions, but will obviously work best on low-dimensional lattices, which have a smaller coordination number.

Let us write $\left[\hat{H}, \hat{O}_\alpha\right] = \sum_{\alpha'} h_{\alpha,\alpha'}\hat{O}_{\alpha'}$ and substitute this into Eq. (16). We get

$$\hat{d}^\dagger_\sigma(t+\Delta t) = \sum_\alpha a_\alpha(t)\,\hat{O}_\alpha + i\Delta t\sum_{\alpha,\alpha'} a_\alpha(t)\,h_{\alpha,\alpha'}\hat{O}_{\alpha'}. \tag{17}$$

Noticing that $\hat{d}^\dagger_\sigma(t+\Delta t) = \sum_\alpha a_\alpha(t+\Delta t)\,\hat{O}_\alpha$ according to Eq. (14) and the expression of $\hat{d}^\dagger_\sigma(t+\Delta t)$ is unique due to our definition of basis operators, we finally obtain the recurrence relation

$$a_\alpha(t+\Delta t) = a_\alpha(t) + i\Delta t\sum_{\alpha'} h_{\alpha',\alpha}a_{\alpha'}(t). \tag{18}$$

By using Eq. (18), we can in principle obtain the coefficients $a_\alpha(t)$ at arbitrary times by an iterative procedure: we begin from an input $a_\alpha(t=0)$ which depends on the operator we wish to evaluate, and advance by a sequence of time steps of size Δt.

We must store all nonzero coefficients $a_\alpha(t)$ along with their corresponding $\hat{O}_\alpha$ at time t in order to compute $a_\alpha(t+\Delta t)$. This demands that the number of nonzero coefficients remain manageable. Fortunately, at $t = 0$ only a single nonzero coefficient is needed to express $\hat{d}^\dagger_\sigma$ (assuming that we choose $\hat{d}^\dagger_{j,\sigma}$ as one of our $\hat{\omega}^i_j$). In a geometric picture, one could say that our target $\hat{d}^\dagger_\sigma(t)$ begins at $t = 0$ exactly on an axis of the operator space at the initial time, and the super operator $[\hat{H}_+,]$ acting on $\hat{d}^\dagger_\sigma$ is quite inefficient at generating new nonzero dimensions. This property guarantees that our algorithm be extremely fast at short times. This property can only

be taken care of within the Heisenberg picture: in the Schrödinger picture, the operator $\hat{H}_+$ acting on a unit basis vector (which is not an eigenstate of the Hamiltonian or extremely local) will immediately generate an infinite number of additional terms, stemming from the infinite number of terms in $\hat{H}_+$. This difference between the two pictures is what makes the Heisenberg picture a far more efficient one to study real time dynamics within the NOM. This is understandable, since in the Heisenberg picture we are restricting our focus to a single observable once a time, while in the Schrödinger picture obtaining the quantum state is equivalent to obtaining all possible observables and should in general be harder.

C. The truncation scheme

While the number of nonzero $a_\alpha(t)$ is always finite, it also increases exponentially as the operator is propagated to longer times. To keep the iterative process feasible, we must limit the number of pairs $\left(a_\alpha, \hat{O}_\alpha\right)$ that are stored in memory. When the number of stored pairs exceeds a given value (which we will denote by M), we perform a truncation and throw out some number of the least important $\left(a_\alpha, \hat{O}_\alpha\right)$. The determination of the relative significance of the $\left(a_\alpha, \hat{O}_\alpha\right)$ at each step, i.e., the truncation scheme, is critical: for our purposes, a good algorithm is needed to allow the algorithm to accurately describe $I(t)$ at long times.

To proceed in deriving an optimal truncation scheme for the current, let us substitute the expansion for $\hat{d}_\sigma^\dagger(t)$ into Eq. (9) to obtain an expression for the current:

$$I(t) = 2\sqrt{\frac{\Gamma}{\pi}} \sum_\alpha \mathrm{Im}\left\{a_\alpha(t)\left\langle \hat{O}_\alpha \hat{c}_{-\sigma}\right\rangle\right\}. \tag{19}$$

In considering this equation, an immediate and naive idea might be to relate the magnitude $\left|\mathrm{Im}\left\{a_\alpha(t)\left\langle \hat{O}_\alpha \hat{c}_{-\sigma}\right\rangle\right\}\right|$ to the significance of $\left(a_\alpha, \hat{O}_\alpha\right)$. However, this idea fails, since it leads to an underestimation of the importance of $|a_\alpha(t)|$, which has an *inheritable* significance. To see this, one should consider the fact that in the iterative relation Eq. (18), a coefficient $a_\alpha(t)$ with a large magnitude also has an important contribution to $a_{\alpha'}(t+\Delta t)$. On the other hand, a small coefficient $|a_\alpha(t)| \sim 0$ can generally be thrown out, since its contribution to $a_{\alpha'}(t+\Delta t)$ is limited by

$$\begin{aligned} &\left|\delta_{\alpha,\alpha'} a_\alpha(t) + i\Delta t \cdot h_{\alpha,\alpha'} a_\alpha(t)\right| \\ &\le \delta_{\alpha,\alpha'} \left|a_\alpha(t)\right| + \Delta t \left|h_{\alpha,\alpha'}\right| \left|a_\alpha(t)\right|, \end{aligned} \tag{20}$$

where the second term vanishes in the limit $\Delta t \to 0$ (since $|h_{\alpha,\alpha'}|$ is bounded). In the other words, if $|a_\alpha(t)|$ is very small, throwing out $\left(a_\alpha, \hat{O}_\alpha\right)$ has no effect on the current at the subsequent time. However, a coefficient with small $\left|\mathrm{Im}\left\{a_\alpha(t)\left\langle \hat{O}_\alpha \hat{c}_{-\sigma}\right\rangle\right\}\right|$ cannot be safely thrown out, since it may have a significant contribution to $I(t+\Delta t)$ even though its contribution to $I(t)$ is essentially zero.

With this in mind, it is clear that using $|a_\alpha(t)|$ as our measure of significance is reasonable. However, it also has the disadvantage of not being optimized specifically to the current. Therefore, it may be better to give weight to the contributions of both $|a_\alpha(t)|$ and $\left|\mathrm{Im}\left\{a_\alpha(t)\left\langle \hat{O}_\alpha \hat{c}_{-\sigma}\right\rangle\right\}\right|$. At short times, it is easy to see that the value of $|a_\alpha(t)|$ fluctuates strongly with different α (for instance, consider $|a_\alpha(0)|$), such that $|a_\alpha(t)|$ is a more important measure than $\left|\mathrm{Im}\left\{a_\alpha(t)\left\langle \hat{O}_\alpha \hat{c}_{-\sigma}\right\rangle\right\}\right|$. At long times, however, we find that the value of the contributing $|a_\alpha(t)|$ at different α is of similar size, a fact which may be understandable as a kind of thermalization of $\hat{d}_\sigma^\dagger(t)$ in the operator space. This leads to $\left|\mathrm{Im}\left\{a_\alpha(t)\left\langle \hat{O}_\alpha \hat{c}_{-\sigma}\right\rangle\right\}\right|$ being more important at long times. In practice, we have used the weight function

$$W_\alpha(t) = |a_\alpha(t)| + \gamma e^{\beta t}\left|\mathrm{Im}\left\{a_\alpha(t)\left\langle \hat{O}_\alpha \hat{c}_{-\sigma}\right\rangle\right\}\right|, \tag{21}$$

where $\gamma, \beta > 0$ are numerical parameters and the choice of their value (which should affect the performance of the algorithm but not the physical result) is decided empirically. After each time step, we arrange the current set of stored operators and coefficient $\left(a_\alpha, \hat{O}_\alpha\right)$ in descending order according to their respective weights $W_\alpha(t)$, and keep the M pairs $\left(a_\alpha, \hat{O}_\alpha\right)$ with the largest W_α. The remaining pairs are discarded. Our experience suggests that this truncation scheme performs far better at long times than the more general alternative truncation scheme $W_\alpha(t) = |a_\alpha(t)|$, which is not specifically tailored to the current (see Fig. 5 and the discussion in Appendix A). It is worth of mentioning that, if choosing $W_\alpha(t) = |a_\alpha(t)|$, we can obtain the current for any possible values of voltage bias in a single calculation, which saves the computational time.

D. Evaluating the expectation value

To obtain the current as expressed in Eq. (19), we need to calculate the expectation value $\left\langle \hat{O}_\alpha \hat{c}_{-\sigma}\right\rangle$ with respect to the initial state. According to the definition of basis operators, this requires evaluating expectation values of the form

$$\left\langle \prod_{j=-1}^{\infty} \hat{\omega}_j^{\alpha_j} \hat{c}_{-\sigma} \right\rangle. \tag{22}$$

Since $\hat{\omega}_j^{\alpha_j}$ is a product of second quantization operators, Eq. (22) can be expanded using Wick's theorem. And we

are able to calculate the contraction of an arbitrary pair of field operators.

There are two kinds of nonzero contractions in Eq. (22), which are $\left\langle \hat{d}^{\dagger}_{n\sigma}\hat{d}_{n'\sigma}\right\rangle$ and $\left\langle \hat{d}^{\dagger}_{n\sigma}\hat{c}_{-\sigma}\right\rangle$. Using the initial condition of subsection III A, a tedious but straightforward calculation gives

$$\left\langle \hat{d}^{\dagger}_{n\sigma}\hat{d}_{n'\sigma}\right\rangle = \sum_{m=0}^{\infty}\frac{u_{nm}u_{n'm}}{2d_m}\left\{\int_{\frac{D}{2\Lambda^{m+1}}}^{\frac{D}{2\Lambda^{m}}} d\epsilon\left[f_L(\epsilon)+f_R(\epsilon)\right] + (-1)^{n+n'}\int_{-\frac{D}{2\Lambda^{m}}}^{-\frac{D}{2\Lambda^{m+1}}} d\epsilon\left[f_L(\epsilon)+f_R(\epsilon)\right]\right\} \tag{23}$$

and

$$\langle \hat{d}^{\dagger}_{n\sigma}\hat{c}_{-\sigma}\rangle = \sum_{m=0}^{\infty}u_{nm}\sqrt{\frac{1}{d_m}} \left[\int_{\frac{D}{2\Lambda^{m}}}^{\frac{D}{2\Lambda^{m}}} d\epsilon + (-1)^{n}\int_{-\frac{D}{2\Lambda^{m}}}^{-\frac{D}{2\Lambda^{m+1}}} d\epsilon\right] \left[e^{-i\epsilon t}\frac{f_L(\epsilon)-f_R(\epsilon)}{2}\right], \tag{24}$$

where $f_\alpha(\epsilon)=\theta(\mu_\alpha-\epsilon)$ is the Fermi distribution, $d_m=\frac{D}{2}\left(\frac{1}{\Lambda^m}-\frac{1}{\Lambda^{m+1}}\right)$ the width of the m-th discretized energy bin, and u_{nm} a set of orthogonal coefficients in the Wilson transformation. u_{nm} is generated by the recurrence relation

$$u_{n+1,m}=\frac{1}{t_n}\left(\frac{D(1+\Lambda)}{4\Lambda^{m+1}}u_{nm}-t_{n-1}u_{n-1,m}\right), \tag{25}$$

with the initial conditions $u_{0m}=\frac{1}{\sqrt{2}}\sqrt{1-\Lambda^{-1}}\Lambda^{-m/2}$ and $u_{1m}=\frac{1}{\sqrt{2}}\sqrt{1-\Lambda^{-3}}\Lambda^{-3m/2}$. A special case is $\left\langle \hat{d}^{\dagger}_{n\sigma}\hat{d}_{n'\sigma}\right\rangle=\frac{1}{2}\delta_{n,n'}$ for even $(n+n')$.

There are four numerical (as opposed to physical) parameters in the algorithm: the time interval Δt, the maximum number of stored coefficients M, and the two parameters γ and β which define the truncation weight function W_α. Our algorithm becomes numerically exact in the limit $M\to\infty$ and $\Delta t\to 0$, regardless of γ and β. To obtain convergence, we start from an initial guess $(\Delta t, M)$ for these values and calculate the current $I(t)_{(\Delta t,M)}$. We then set $\Delta t\to\Delta t/2$ and $M\to 2M$ and repeat the calculation to obtain $I(t)_{(\Delta t/2,2M)}$. The difference $\left|I(t)_{(\Delta t,M)}-I(t)_{(\Delta t/2,2M)}\right|$ provides us with an approximate estimate of the error, and we can now iterate this procedure until the error is small enough for our requirements, at which point we say that convergence is reached.

This concludes our discussion of the algorithm. In the next section, we will present several examples and comparisons with other methods.

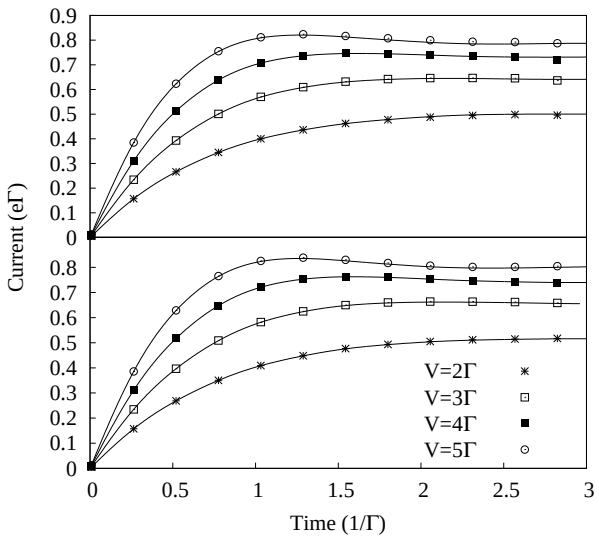

Figure 1. The time dependent current $I(t)$ computed at $\Lambda=1.02$ (represented by solid lines) and at $\Lambda=1.2$ (represented by symbols) at several different bias voltages V and two different interaction strengths U. The results at $\Lambda=1.02$ coincide with those at $\Lambda=1.2$, indicating that the latter is small enough to attain convergence of the discretization of reservoirs at these parameters and timescales. (Top panel) The interaction strength is $U=\Gamma$. (Bottom panel) The interaction strength is $U=0.01\Gamma$.

IV. RESULT AND DISCUSSION

A. Numerical parameters and convergence

We set the bandwidth of the reservoirs to $D=20\Gamma$ and calculate $I(t)$ at the particle-hole symmetric point $\epsilon_d=-U/2$ for different interaction strengths U and bias voltages V. The choice of the truncation parameters γ and β is empirical. We have tried different values in order to minimize the error of $I(t)$ at a given time for given Δt and M, and found that $\gamma=2$ and $\beta=3$ is a good choice for a wide range of parameters (see Appendix A for more detail). With the truncation scheme we have proposed, computation time is efficiently reduced to a manageable level (see Appendix B for more detail): in practice we find that $M=40000$ for $U=4.0\Gamma$ or $M=60000$ for the other values of U and $\Delta t=0.008/\Gamma$ provide a good estimate of $I(t)$ for the parameters treated in this paper. In general, however, we find that to obtain accurate results at longer times a larger M is required, such that the computational scaling in the propagation time t is in practice substantially more than linear. In the general case, this is of course a universal problem in all numerically exact methods. We briefly mention that under certain conditions it can be overcome by reduced dynamics techniques,[56,59,60] but this is beyond the scope of this paper.

An important problem that has been mentioned in sec. II is that the Wilson chain is not a thermal reser-

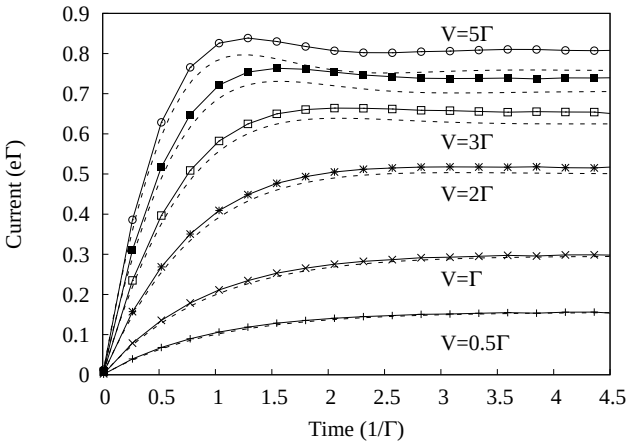

Figure 2. The current $I(t)$ at weak interaction strength $U = 0.01\Gamma$ and for a range of bias voltages $\frac{V}{\Gamma} = \frac{1}{2}, 1, 2, 3, 4, 5$. We compare results calculated with the NOM at finite bandwidth, $D = 20$ (symbols connected by solid lines), with results calculated by second order perturbation theory at infinite bandwidth, $D \to \infty$ (dashed lines).

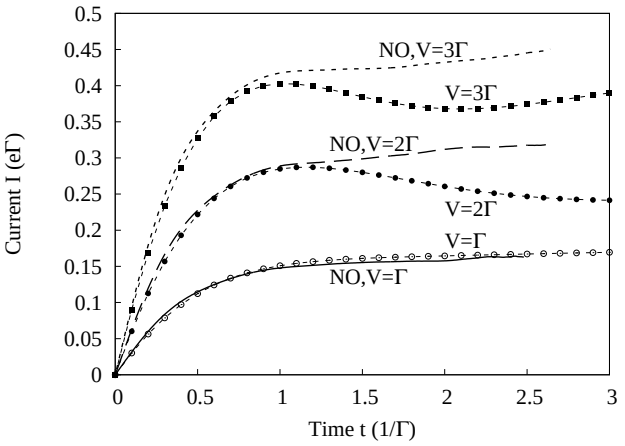

Figure 3. The current $I(t)$ at intermediate interaction strength $U = 4\Gamma$ for several different bias voltages $\frac{V}{\Gamma} = 1, 2, 3$. We compare results calculated with the NOM at finite bandwidth, $D = 20$ (symbols connected by solid lines), with results calculated by second order perturbation theory at infinite bandwidth, $D \to \infty$ (dashed lines).

voir at $\Lambda > 1$. We circumvent this issue by converging the data with the limit where $\Lambda \to 1$ for finite times. In Fig. 1, we present the results at different Λ for different interaction strengths and bias voltages. We find that $\Lambda = 1.2$ and $\Lambda = 1.02$ give comparable results, indicating that the data is converged.

B. Weak and intermediate interactions

Having established that the NOM converges to a well-defined answer, we now continue to argue that this answer is correct. This will be done by performing a set comparisons with trustworthy analytical and numerical results. We begin at the limit of weak interaction. For noninteracting (quadratic) systems, the NOM has previously been discussed in the literature and was shown to agree perfectly with the results of exact diagonalization.[77] We therefore begin with weakly interacting systems at interaction strength $U = 0.01\Gamma$, where second order perturbation theory in U may be expected to work well.

In Fig. 2 we present a comparison between the NOM at a bandwidth of $D = 20\Gamma$ and perturbation theory. The perturbation theory data comes from ref. 18, where the flow equation technique (which is equivalent at steady state to the Keldysh technique of ref. 78) was applied to the Anderson impurity model at the wide band limit $D \to \infty$. As expected, the two data sets converge at low voltages, e.g., at $V = 0.5\Gamma$ and $V = \Gamma$. We also find moderate deviation of our results from the perturbation theory at high bias voltage, where one might expect the bandwidth to be more important. In the presence of interactions, the bandwidth affects the current even when the transport window is narrower than the bandwidth ($V < D$): due to inelastic scattering effects, levels in the bands are effectively mixed. We note that the limit $D/\Gamma \to \infty$ is not reachable by our algorithm, and in general the computational time increases significantly as we increase the bandwidth D/Γ. In essence, a large bandwidth acts oppositely to the beneficial effects of the logarithmic discretization with $\Lambda > 1$. The logarithmic discretization speeds up the algorithm by transforming the model into a Wilson chain in which the coupling between adjacent sites decreases exponentially with distance from the impurity. The vanishing coupling far away from the impurity site effectively suppresses the growth of the operator space in the iterative process, thereby reducing the computational time (see Fig. 7 and the discussion in Appendix B). As the bandwidth D increases, the coupling grows according to Eq. (6), raising the coefficients $|a_\alpha(t)|$ and yielding slow convergence.

In Fig. 3, we further compare our method with perturbation theory at an intermediate interaction strength of $U = 4\Gamma$. Interestingly, the numerical curves continue to fit well with the perturbative theory at low bias voltages, but deviate from it qualitatively at high bias voltage. This suggests that the second order perturbation theory still works well at $U = 4\Gamma$ and low voltage. At higher bias voltages the deviation may be attributed to either the failure of the perturbative approximation or the difference in bandwidth. The inelastic scattering at $U = 4\Gamma$ is stronger than that at $U = 0.01\Gamma$, such that the finite D affects the current to a greater degree.

C. Strong interactions

Finally, we study the current $I(t)$ within the strong coupling regime by considering $U = 8\Gamma$. In

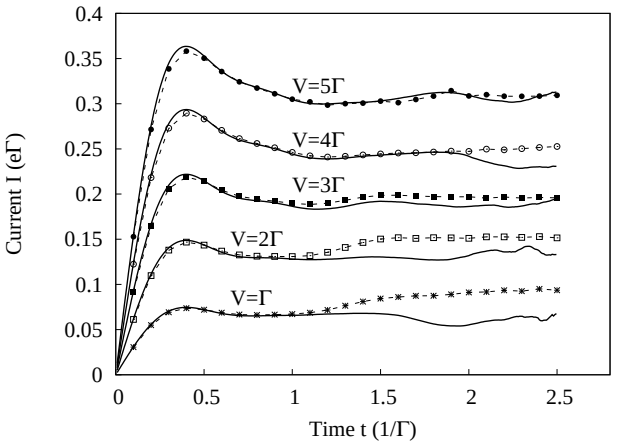

Figure 4. The current $I(t)$ at a large interaction strength $U = 8\Gamma$ and several different bias voltages $\frac{V}{\Gamma} = 1, 2, 3, 4, 5$, as calculated by the NOM (solid lines) and the QMC method of ref. 55 (symbols connected by dashed lines).

nonequilibrium—that is, beyond linear response in the voltage—exact analytical results are not available. Linear response is thought to be valid for voltages approximately limited by the Kondo temperature $T_K \sim e^{-U/\Gamma}$, and therefore quite small. We compare with numerically exact QMC results at a low but finite temperature of $T = 0.1\Gamma$, in comparison with $T = 0$ in the NOM. The short time behavior is accessible with continuous time quantum Monte Carlo techniques,[39,51] at least for temperatures which are not too low. Newer bold-line techniques[55,79] allow access to longer times and lower temperatures. We have compared the QMC results with similar at $T = 0.2\Gamma$ (not shown) and verified that within the timescales accessed here, the effect of the finite temperature is small. Also, within QMC we take soft band edges, which are defined by a product of Fermi functions having width $\nu = 0.1\Gamma$, as in ref. 51. The QMC simulations are otherwise performed at the same parameters as the NOM.

The current $I(t)$ at different bias voltages up to $\Gamma t = 2.5$, as calculated by both methods, is displayed in Fig. 4. The results are consistent at the highest voltage $V = 5\Gamma$. However, even at $V = 5\Gamma$, it is clear that the NOM gives a slightly larger current around the first peak at $\Gamma t \sim 0.5$, which can be attributed to the difference in temperature and band shape. At lower voltages the two methods exhibit good agreement at short times, but deviate significantly from each other at longer times. Though steady state is not reached here, NOM appears to predict a smaller steady state current than QMC. We do not believe that this can be explained by the difference in temperatures, since from the previously mentioned check we find that reducing the temperature in QMC leads to the opposite trend. QMC studies similarly suggest that the importance of the band cutoff width ν is relatively unimportant at these parameters. The rise in current at low voltages may be associated with the formation of Kondo resonances at the chemical potentials,[33] and the failure of the NOM at these parameters indicates a problem either with the Wilson mapping (which implies low resolution at high energies) or with our truncation scheme. In either case, it requires further investigation which will be left to future studies.

V. CONCLUSIONS

In summary, we have developed the numerical operator method, or NOM, and applied it to the study of the real time dynamics of strongly-correlated quantum impurity models in nonequilibrium. This is a notoriously difficult problem to which many techniques have been applied. Our method is distinguished by three important features, which we briefly outline below.

First, in the mapping of the reservoirs onto 1D chains, any discretization scheme is supported. This is similar to DMRG, but differs from NRG; in QMC the issue of mapping onto a 1D chain need not arise. It also allows us to efficiently take the limit $\Lambda \to 1$ when using the Wilson mapping.

Second, our method revolves around the solution of the Heisenberg equation of motion. We carefully select a basis in the operator space such that the superoperator $[\acute{H}, \ldots]$ acting on our chosen observable in this basis generates only a small number of terms. This allows us to effectively set the length of the reservoir chains to infinity, thus circumventing the finite-size scaling problems encountered by other (non-QMC) numerical techniques.

Third, we provide a truncation scheme (see Eq. (21)) suited to the characteristics of the solution of the Heisenberg equation and optimized for specific observables. Therefore, our algorithm is extremely fast and accurate in the short time limit, and additionally provides a controllable scheme for obtaining high quality approximations of physical observables at longer times. The downside of this is that our method only addresses a single observable per computation: to calculate an additional observable, the entire time evolution process must be repeated. However, in many cases, only one or very few observables are of interest.

We note that while these features are also shared by tDMRG schemes formulated for matrix product operators,[71] our truncation scheme is different and does not rely on the assumption of low entanglement, which may not be appropriate for nonequilibrium dynamics.

As an example, we apply our method to the real time dynamics of transport through the nonequilibrium Anderson impurity model. We calculate the time dependence of the current in a wide range of interaction strengths and bias voltages going far beyond the linear response regime in both quantities. We show that at small interaction strengths, our results coincide with perturbation theory in the interaction. We further compare our results with QMC data at a large interaction strength

for which no analytical method is known to be applicable, and find good agreement as long as Kondo physics does not come into play.

We have therefore established the NOM as a reliable new formalism for exploring nonequilibrium transport properties in the impurity models over a wide range of parameters and at zero temperature. We expect to generalize our method to more complicated quantum impurity models and to two-time correlation functions in the future, and further analyze its advantages and limitations. In particular, a comparison with tDMRG is in order, and the relative merits of the NOM basis and the truncation scheme as opposed to those of matrix product operator algorithms should be studied in detail. Finally, modifications to DMRG which have allowed for the study of finite temperatures[80–82] and open systems coupled to Markovian baths[83–85] should also be usable within the NOM.

ACKNOWLEDGMENTS

P. W. and S. X. were supported by the NSFC (Grants No. 11304280 and No. 71103161). G. C. is grateful to the Yad Hanadiv-Rothschild Foundation for the award of a Rothschild Postdoctoral Fellowship, and acknowledges NSF CHE-1213247 and NSF DMR 1006282. QMC implementations were based on the ALPS[86] libraries.

Appendix A: Convergence of the results

A self-consistent method for determining the accuracy of the method is necessary for serious applications and will need to be developed in the future. At this stage, we can roughly estimate the truncation error for different truncation schemes and the finite-Δt error by increasing the number M of coefficients kept or by decreasing Δt, respectively, and observing how the results vary, since at the limit of $M \to \infty$ and $\Delta t \to 0$ the computation always becomes exact.

Fig. 5 shows how the currents at different times change when M is increased for a set of different truncation schemes. As discussed in the last paragraph of subsection III C, the truncation schemes that we consider are spanned by the pair of positive numbers (γ, β). When considering the shortest propagation time shown, $t = 1.6/\Gamma$ (see panel (a)), all five truncation schemes with different (γ, β) converge to similar values at relatively low M. In particular, as discussed in the subsection III C, the red and black lines denote the two most successful truncation schemes. By comparing the differences between these two results, the truncation error may be judged to be approximately $0.01/0.3 \approx 3.3\%$. We note that this is not a rigorous analysis and that an algorithm for self-consistently evaluating the truncation errors within the method remains an important goal for future work.

At $t = 2.0/\Gamma$ (panel (b)), we clearly see that the truncation error is strongly suppressed as γ increases from

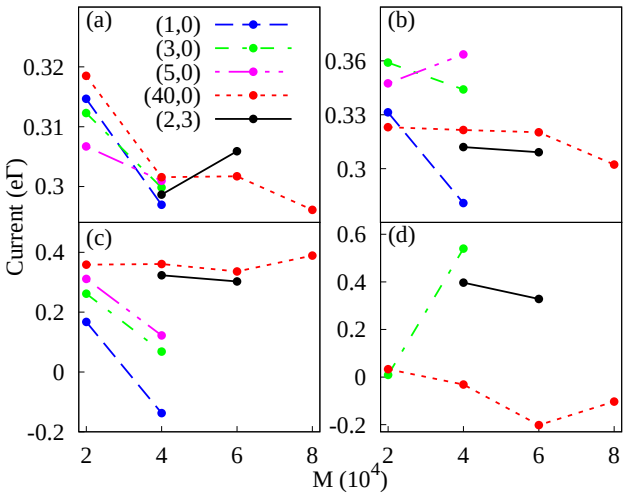

Figure 5. [Color online] The change of currents at the times (a) $t = 1.6/\Gamma$, (b) $t = 2.0/\Gamma$, (c) $t = 2.2/\Gamma$ and (d) $t = 2.56/\Gamma$ when as a function of M, the number of coefficients kept. The different lines illustrate the dependence on the truncation scheme, which is indicated by the pair (γ, β) as defined in Eq. (21) of the manuscript. The other parameters are the same as those of the $V = 5\Gamma$ curve in Fig. 4 of the manuscript.

$\gamma = 1$ (the blue) to $\gamma = 40$ (the red), reflecting the fact that the weight of the expectation value should be increasingly significant in the truncation scheme as t grows larger. At a still longer time $t = 2.2/\Gamma$, the truncation schemes with small γ (the blue, green and pink lines) clearly fail, exhibiting relative errors exceeding 100%. Only the truncation schemes with $\gamma = 40, \beta = 0$ (red line) and $\gamma = 2, \beta = 3$ (black line) continue to provide consistent results. The black $(2, 3)$ scheme is particularly advantageous, and this advantage is even more significant at the largest time $t = 2.56/\Gamma$ (panel (d)). In this case,all other schemes fail, and the $(40, 0)$ scheme results in an unphysical result (negative current). We conclude that the weight of the expectation value in the truncation scheme should be more significant at a larger time. For this reason, an exponential weight function $\gamma e^{\beta t}$ works better than a constant weight function ($\beta = 0$) or the truncation scheme which neglects the expectation value ($\gamma = 0$).

We illustrate the convergence of results with decreasing Δt in Fig. 6, using the truncation scheme defined by $\gamma = 2, \beta = 3$. While this is not a complete analysis, we can see that the error caused by a finite Δt in the range $\Delta t \leq 0.008/\Gamma$ increases slightly as t increases. However, even at $t = 2.1/\Gamma$, nearly the largest time that we reach, the finite Δt error remains around $0.003/0.3 = 1\%$, substantially less than the truncation error. The truncation error is therefore the dominant source of error in our algorithm. We also note that the error increases very fast as Δt goes beyond $0.01/\Gamma$, especially for the results at large t.

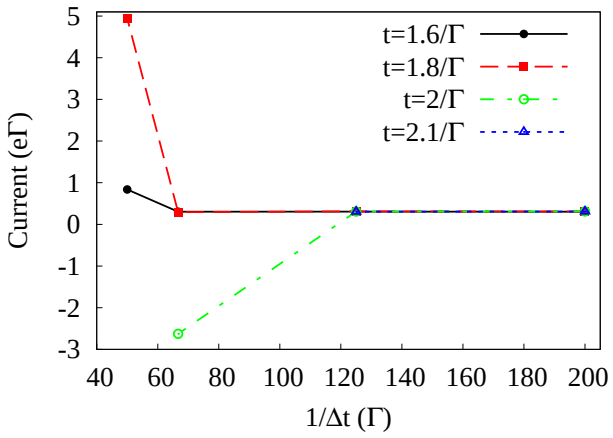

Figure 6. [Color online] The dependence of the current on the inverse of the time discretization $1/\Delta t$ at different times. The other parameters are as in Fig. 4 for $V = 5\Gamma$.

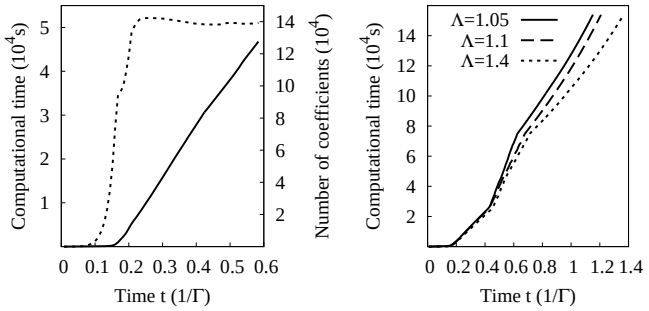

Figure 7. (Left panel) The number of basis operators in the memory before truncation (dashed line) and the elapsed CPU time (solid line) as a function of t in a typical calculation. (Right panel) The comparison of the elapsed CPU time at different Λ. All the other parameters are taken the same as those of Fig. 4, $V = 5\Gamma$ curve.

Appendix B: Computational cost

The computational cost strongly depends on the interaction strength U, the time step Δt, the number of stored coefficients M, the discretization parameter Λ, and the truncation parameter γ. Increasing U significantly raises the computation time. In the noninteracting or weakly-interacting regime, the number of non-zero $a_\alpha(t)$ increases approximately linearly with t, but exponentially with t in the strongly-interacting regime. It is therefore more difficult to obtain a converged result at large U. Reducing Δt or increasing M obviously raises the computational cost, but also improves the precision of results. In practice, a balance between the computational cost and the precision must be taken carefully. The coupling between two neighboring sites of the Wilson chain scales approximately as $\Lambda^{-n/2}$. Increasing Λ reduces the coupling between sites far from the impurity site, thus effectively suppressing the growth of the active operator space and leading to the reduction of the computational cost. γ affects the computation time in a complex way: with $\gamma = 0$, one avoids calculating the expectation value of the basis operator at each step, and can obtain the currents at arbitrary voltage in a single calculation since the Heisenberg equation is independent to the voltage bias. Taking $\gamma = 0$ therefore saves a lot of computation time; however, this only works in the non-interacting or weakly-interacting region. In the strongly-interacting region, taking $\gamma = 0$ leads to a very slow convergence at large t and is not feasible in general.

In the left panel of Fig. 7, we have chosen one particular dataset and plotted the number of basis operators kept in memory before truncation at each step along with the elapsed CPU time. The parameters taken are $U = 8\Gamma$, $M = 60000$, $\tau = 0.008/\Gamma$, $\gamma = 2$ and $\beta = 3$. We see that the truncation becomes necessary, i.e., the number of operators before truncation is beyond M, at $t \sim 0.15/\Gamma$. This is also the typical time scale at which the truncation begins to come into play in Fig. 1-4. The number of basis operators before truncation, which roughly corresponds to the computational cost at each step, saturates at a value ~ 140000 within a short time $t \sim 0.2/\Gamma$. The computational time scales sub-linearly in t for very short times (when the number of operators in the basis is still small), and becomes approximately linear in t once the basis growth becomes limited by M. The right panel of Fig. 7 shows the computational time at different Λ. We see that the computational time is reduced as Λ increases, coinciding with the above analysis. Roughly speaking, the data of Fig. 1-4, were obtained from calculations taking between a few days to over 10 days on a single core. The interaction strength affected the total computation time more strongly than any other parameter.

* wangpei@zjut.edu.cn

[1] A. Aviram and M. A. Ratner, Chem. Phys. Lett. **29**, 277 (1974).
[2] J. Jortner and M. Ratner, *Molecular Electronics* (Blackwell Science Inc., New York, 1997).
[3] C. Joachim, J. K. Gimzewski, and A. Aviram, Nature **408**, 541 (2000).
[4] R. M. Metzger, J. Macromol. Sci. Pure Appl. Chem. **A38**, 1499 (2001).
[5] J. R. Heath and M. A. Ratner, Physics Today **56**, 43 (2003).
[6] C. Joachim and M. A. Ratner, Proc. Natl. Acad. Sci. **102**, 8801 (2005).
[7] S. Datta, *Electronic Transport in Mesoscopic Systems* (Cambridge UniversityPress, 1997).
[8] D. Goldhaber-Gordon, H. Shtrikman, D. Mahalu,

D. Abusch-Magder, U. Meirav, and M. A. Kastner, Nature **391**, 156 (1998).
[9] Y. Imry, *Introduction to Mesoscopic Physics, 2nd ed.* (Oxford University Press, Oxford, 2002).
[10] A. Asamitsu, Y. Tomioka, H. Kuwahara, and Y. Tokura, Nature **388**, 50 (1997).
[11] S. Iwai, M. Ono, A. Maeda, H. Matsuzaki, H. Kishida, H. Okamoto, and Y. Tokura, Physical Review Letters **91**, 057401 (2003).
[12] M. Liu, H. Y. Hwang, H. Tao, A. C. Strikwerda, K. Fan, G. R. Keiser, A. J. Sternbach, K. G. West, S. Kittiwatanakul, J. Lu, S. A. Wolf, F. G. Omenetto, X. Zhang, K. A. Nelson, and R. D. Averitt, Nature **487**, 345 (2012).
[13] S. Datta, *Electronic Transport in Mesoscopic Systems* (Cambridge University Press, Cambridge, 1995).
[14] M. Plihal, D. C. Langreth, and P. Nordlander, Physical Review B **71**, 165321 (2005).
[15] H. Haug and A. P. Jauho, *Quantum kinetics in transport and optics of semiconductors* (Springer Verlag, 2008).
[16] C. Karrasch, S. Andergassen, M. Pletyukhov, D. Schuricht, L. Borda, V. Meden, and H. Schoeller, EPL (Europhysics Letters) **90**, 30003 (2010).
[17] M. Pletyukhov, D. Schuricht, and H. Schoeller, Physical Review Letters **104**, 106801 (2010).
[18] P. Wang and S. Kehrein, Physical Review B **82**, 125124 (2010).
[19] D. W. H. Swenson, T. Levy, G. Cohen, E. Rabani, and W. H. Miller, The Journal of Chemical Physics **134**, 164103 (2011).
[20] D. M. Kennes and V. Meden, Physical Review B **85**, 245101 (2012).
[21] D. M. Kennes, S. G. Jakobs, C. Karrasch, and V. Meden, Physical Review B **85**, 085113 (2012).
[22] M. Pletyukhov and H. Schoeller, Physical Review Letters **108**, 260601 (2012).
[23] B. Li, E. Y. Wilner, M. Thoss, E. Rabani, and W. H. Miller, The Journal of Chemical Physics **140**, 104110 (2014).
[24] L. Perfetti, P. A. Loukakos, M. Lisowski, U. Bovensiepen, H. Berger, S. Biermann, P. S. Cornaglia, A. Georges, and M. Wolf, Physical Review Letters **97**, 067402 (2006).
[25] T. Kinoshita, T. Wenger, and D. S. Weiss, Nature **440**, 900 (2006).
[26] L. E. Sadler, J. M. Higbie, S. R. Leslie, M. Vengalattore, and D. M. Stamper-Kurn, Nature **443**, 312 (2006).
[27] I. Bloch, Science **319**, 1202 (2008).
[28] P. Calabrese and J. Cardy, Physical Review Letters **96**, 136801 (2006).
[29] C. Kollath, A. M. Läuchli, and E. Altman, Physical Review Letters **98**, 180601 (2007).
[30] M. Eckstein, M. Kollar, and P. Werner, Physical Review Letters **103**, 056403 (2009).
[31] M. Schiró and M. Fabrizio, Physical Review Letters **105**, 076401 (2010).
[32] P. Werner, T. Oka, M. Eckstein, and A. J. Millis, Physical Review B **81**, 035108 (2010).
[33] G. Cohen, E. Gull, D. R. Reichman, and A. J. Millis, Physical Review Letters **112**, 146802 (2014).
[34] Y. Meir and N. S. Wingreen, Physical Review Letters **68**, 2512 (1992).
[35] A.-P. Jauho, N. S. Wingreen, and Y. Meir, Physical Review B **50**, 5528 (1994).
[36] R. Bulla, T. A. Costi, and T. Pruschke, Reviews of Modern Physics **80**, 395 (2008).
[37] A. C. Hewson, *The Kondo Problem to Heavy Fermions* (Cambridge University Press, Cambridge, 1993).
[38] E. Gull, P. Werner, O. Parcollet, and M. Troyer, EPL (Europhysics Letters) **82**, 57003 (2008).
[39] E. Gull, A. J. Millis, A. I. Lichtenstein, A. N. Rubtsov, M. Troyer, and P. Werner, Reviews of Modern Physics **83**, 349 (2011).
[40] D. Zgid, E. Gull, and G. K.-L. Chan, Physical Review B **86**, 165128 (2012).
[41] M. Ganahl, P. Thunström, F. Verstraete, K. Held, and H. G. Evertz, Physical Review B **90**, 045144 (2014).
[42] Y. Lu, M. Höppner, O. Gunnarsson, and M. W. Haverkort, Physical Review B **90**, 085102 (2014).
[43] F. B. Anders and A. Schiller, Physical Review Letters **95**, 196801 (2005).
[44] F. B. Anders, Journal of Physics: Condensed Matter **20**, 195216 (2008).
[45] L. Mühlbacher and E. Rabani, Physical Review Letters **100**, 176403 (2008).
[46] S. Weiss, J. Eckel, M. Thorwart, and R. Egger, Physical Review B **77**, 195316 (2008).
[47] J. Jin, X. Zheng, and Y. J. Yan, The Journal of chemical physics **128**, 234703 (2008).
[48] T. Schmidt, P. Werner, L. Mühlbacher, and A. Komnik, Cond. Mat. , 0808.0442 (2008).
[49] L. G. G. V. Dias da Silva, F. Heidrich-Meisner, A. E. Feiguin, C. A. Büsser, G. B. Martins, E. V. Anda, and E. Dagotto, Physical Review B **78**, 195317 (2008).
[50] F. Heidrich-Meisner, A. E. Feiguin, and E. Dagotto, Physical Review B **79**, 235336 (2009).
[51] P. Werner, T. Oka, and A. J. Millis, Physical Review B **79**, 035320 (2009).
[52] H. Wang and M. Thoss, The Journal of chemical physics **131**, 024114 (2009).
[53] D. Segal, A. J. Millis, and D. R. Reichman, Physical Review B **82**, 205323 (2010).
[54] J. Eckel, F. Heidrich-Meisner, S. G. Jakobs, M. Thorwart, M. Pletyukhov, and R. Egger, New Journal of Physics **12**, 043042 (2010).
[55] E. Gull, D. R. Reichman, and A. J. Millis, Physical Review B **84**, 085134 (2011).
[56] G. Cohen and E. Rabani, Physical Review B **84**, 075150 (2011).
[57] H. Wang, I. Pshenichnyuk, R. Härtle, and M. Thoss, The Journal of Chemical Physics **135**, 244506 (2011).
[58] S. Bedkihal and D. Segal, Physical Review B **85**, 155324 (2012).
[59] G. Cohen, E. Gull, D. R. Reichman, A. J. Millis, and E. Rabani, Physical Review B **87**, 195108 (2013).
[60] G. Cohen, E. Y. Wilner, and E. Rabani, New Journal of Physics **15**, 073018 (2013).
[61] R. Härtle, G. Cohen, D. R. Reichman, and A. J. Millis, Physical Review B **88**, 235426 (2013).
[62] L. Simine and D. Segal, The Journal of Chemical Physics **138**, 214111 (2013).
[63] F. B. Anders, Physical Review Letters **101**, 066804 (2008).
[64] A. Georges and G. Kotliar, Physical Review B **45**, 6479 (1992).
[65] A. Georges, G. Kotliar, W. Krauth, and M. J. Rozenberg, Reviews of Modern Physics **68**, 13 (1996).
[66] G. Kotliar, S. Y. Savrasov, K. Haule, V. S. Oudovenko, O. Parcollet, and C. A. Marianetti, Reviews of Modern Physics **78**, 865 (2006).
[67] M. Žnidarič, T. Prosen, and P. Prelovšek, Physical Review

B **77**, 064426 (2008).
[68] T. Prosen and M. Žnidarič, Journal of Statistical Mechanics: Theory and Experiment **2009**, P02035 (2009).
[69] M. J. Hartmann, J. Prior, S. R. Clark, and M. B. Plenio, Physical Review Letters **102**, 057202 (2009).
[70] M. C. Bañuls, M. B. Hastings, F. Verstraete, and J. I. Cirac, Physical Review Letters **102**, 240603 (2009).
[71] U. Schollwöck, Annals of Physics **326**, 96 (2011).
[72] T. Enss and J. Sirker, New Journal of Physics **14**, 023008 (2012).
[73] P. Wang, The European Physical Journal B **86**, 494 (2013).
[74] P. Wang, Physica E: Low-dimensional Systems and Nanostructures **47**, 141 (2013).
[75] Y. Meir, N. S. Wingreen, and P. A. Lee, Physical Review Letters **70**, 2601 (1993).
[76] A. Rosch, The European Physical Journal B - Condensed Matter and Complex Systems **85**, 1 (2012).
[77] P. Wang, X. Zhao, and L. Tang, The European Physical Journal B **87**, 73 (2014).
[78] T. Fujii and K. Ueda, Physical Review B **68**, 155310 (2003).
[79] E. Gull, D. R. Reichman, and A. J. Millis, Physical Review B **82**, 075109 (2010).
[80] A. E. Feiguin and S. R. White, Physical Review B **72**, 220401 (2005).
[81] S. R. White, Physical Review Letters **102**, 190601 (2009).
[82] E. M. Stoudenmire and S. R. White, New Journal of Physics **12**, 055026 (2010).
[83] M. Zwolak and G. Vidal, Physical Review Letters **93**, 207205 (2004).
[84] F. Verstraete, J. J. García-Ripoll, and J. I. Cirac, Physical Review Letters **93**, 207204 (2004).
[85] A. J. Daley, J. M. Taylor, S. Diehl, M. Baranov, and P. Zoller, Physical Review Letters **102**, 040402 (2009).
[86] B. Bauer, L. D. Carr, H. G. Evertz, A. Feiguin, J. Freire, S. Fuchs, L. Gamper, J. Gukelberger, E. Gull, S. Guertler, A. Hehn, R. Igarashi, S. V. Isakov, D. Koop, P. N. Ma, P. Mates, H. Matsuo, O. Parcollet, G. Pawłowski, J. D. Picon, L. Pollet, E. Santos, V. W. Scarola, U. Schollwöck, C. Silva, B. Surer, S. Todo, S. Trebst, M. Troyer, M. L. Wall, P. Werner, and S. Wessel, Journal of Statistical Mechanics: Theory and Experiment **2011**, P05001 (2011).